Materials Today Communications 22 (2020) 100755

Contents lists available at ScienceDirect

Materials Today Communications

journal homepage: www.elsevier.com/locate/mtcomm

Use of ball mill to prepare nanocellulose from eucalyptus biomass: Challenges and process optimization by combined method

Rafaela R. Ferreira[a], Alana G. Souza[a], Lucas L. Nunes[a], Naresh Shahi[b], Vijaya K. Rangari[c], Derval dos Santos Rosa[a,*]

[a] Centro de Engenharia, Modelagem e Ciências Sociais Aplicadas – CECS/ Universidade Federal do ABC (UFABC), Avenida dos Estados, 5001, CEP: 09210-580, Santo André, SP, Brazil
[b] Integrative Biosciences (IBS) Graduate School of PHD Program, Tuskegee University, AL 26088, USA
[c] Department of Materials Science and Engineering, Tuskegee University, Tuskegee, AL 36088, USA

ARTICLE INFO

Keywords:
Mechanical methods
Cellulose nanostructures
Ball mill
High-intensity ultrasound
Eucalyptus sawdust
Nanoparticles' characterization

ABSTRACT

A combination of mechanical methods was developed to obtain a suspension of nanocellulose (NC) from Eucalyptus sawdust. In this two-step process, the ball milling (1–4 h) was followed by a high-intensity ultrasound (10–30 min) irradiation. The prepared samples were characterized using Fourier-transform infrared spectroscopy, Raman, dynamic and static light scattering, Zeta potential, X-ray diffraction, X-ray photoelectron spectroscopy, Thermogravimetric analysis, Field-emission scanning electron microscopy, and Transmission electron microscopy. The crystallinity was calculated using different methods and compared. The mechanical grinding results in a random and irregular break of the fibers. In a combined method, the ultrasound waves generate more defibrillation and separation of the nanofibers and, consequently, the reduction of fiber diameters. The high-intensity ultrasound promoted an increase in the homogeneity, crystallinity, and electrostatic and thermal stability of the NC suspension. The samples milled for 2 h and 20 min ultrasound irradiation presented the high-efficiency in obtaining NC.

1. Introduction

Cellulose is an environmentally friendly biopolymer derived from natural sources such as forest waste, woody biomass, crops, algae, and microorganisms. Cellulose and its derivatives are sustainable and biodegradable, therefore receiving exceptional attention as a substitute for petrochemical feedstock in polymer industries [1]. More recently, uses of cellulose from the forest residues have been devoted to the isolation of nanocellulose (NC), and Eucalyptus sawdust is one of them. Eucalyptus is a fast-growing wood that covers a larger planted area with approximately 187 million ha in the world [2]. During the processing of eucalyptus, an enormous amount of sawdust is originated, which is rich in lignocellulosic constituents ˜25 – 35 wt.% of lignin, ˜20 – 30 wt.% of hemicellulose and ˜35 – 40 wt.% of cellulose [3]. The residues are often disposing as waste or burning for energy production. It results in high emissions of pollutant gas [4] leads to undesirable environmental consequences.

Nanocellulose is a new class of eco-material with unique properties such as nanoscale dimension, high surface area, high strength, specific modulus, unique morphology, and excellent optical properties [5]. Due to the unique properties of NC, this material is applicable in many fields, such as mechanical reinforcements in composite materials, bioengineering, pharmaceutical, and biomedical technologies [6]. A wide range of applications and products can be developed; therefore, NC is a fascinating next-generation engineering material to researchers and industries.

Several top-down approaches are available for NC isolation, such as chemical, biological, mechanical, and combination of chemical and mechanical [7–9]. However, an environmentally-friendly combination method that does not employ strong acids or toxic reagents has not been widely explored. Various chemical processes are required to transform the lignocellulose rich sawdust into cellulose pulp [10].

Usually, chemical methods are conducted by acid hydrolysis using strong acids, and it is well established [5,11–14]. However, chemicals are always risky to handle, corrosive to the equipment's, and detrimental effect on the environment [5,10]. The enzymatic hydrolysis represents the biological method. This method requires long reaction times, and the cost of enzymes is usually high and also limited uses

* Corresponding author.
E-mail addresses: reis.f@ufabc.edu.br (R.R. Ferreira), alana.gabrieli@ufabc.edu.br (A.G. Souza), lucas.nunes11@fatec.sp.gov.br (L.L. Nunes), nshahi1164@tuskegee.edu (N. Shahi), vrangari@tuskegee.edu (V.K. Rangari), dervalrosa@yahoo.com.br (D.d.S. Rosa).

https://doi.org/10.1016/j.mtcomm.2019.100755
Received 3 August 2019; Received in revised form 28 October 2019; Accepted 5 November 2019
Available online 07 November 2019
2352-4928/

[15,16]. On the other hand, mechanical methods are simple and do not require chemical reagents; this type of method are outstanding due to their high production capacity and low cost [17–19]. The main examples of mechanical methods are ball mill, cryogenic break, and ultrasound.

The ball mill is an environmentally friendly and low-cost technique that is widely applied in the industry all over the world. It consists of a cylindrical shell rotating around its axis, which is partially filled with balls; the energy released from impact and attriction between the balls and the samples converts the particles from micro- to nanoscale [20]. However, some disadvantages include the possibility of contamination, usually ceramic or metal, from grinding medium and container, the formation of irregular shapes, and extended milling and cleaning times [5,21]. The current literature survey shows the frequent uses of planetary ball milling (high-energy ball mill) or shaker mill for obtaining NC, and/or acid solutions during the milling. The planetary ball mill achieves higher rotations and requires much energy; it has very low milling capacity due to the small containers and is not common on an industrial scale [5,17,22]. The tumbler ball mill, which was used in this work, is a very simple process that depends mainly on the time and balls and diameter of the container [21,23,24].

While the ball mill involves friction and shear forces, the ultrasound process applies the use of oscillating power to create hydrodynamic forces of ultrasound [25]. The high intensive waves result in the formation, expansion, and implosion of microscopic gas bubbles when the sample absorbs the energy, and this intense energy decreases the size of the particles [26,27]. However, generally high times or low sample quantity per process need to be used. Aiming to find an environmental process with high efficiency and low cost, researches are combining two or more isolation methods at the same time or in sequence. The combination of mechanical methods, such as ball mill and high-intensity ultrasound have recently been highlighted [22].

The purpose of the study was to develop a combined mechanical method (ball milled and ultrasound) to isolated NC from Eucalyptus sawdust. This method can be extended to large scale production, which is different from the existing literature, is simple, low cost, and commercially attractive. It is important to mention that the production of nanocellulose in a pilot-scale is currently carried out mainly by acid hydrolysis [28,29]. The NCs isolated were characterized by morphological, chemical, physical, and thermal properties. Furthermore, the crystallinity of the NC was compared with XRD, Raman, and FTIR. Therefore, this study aimed to transform Eucalyptus residues as promising sources of high value-added biopolymer (in the NC form).

2. Experimental

2.1. Materials

Eucalyptus citriodora waste (eucalyptus sawdust – ES) was kindly donated after harvesting and cutting at the state of Mato Grosso, Brazil. The composition of the eucalyptus sawdust was ˜33 wt.% of lignin, ˜27 wt.% of hemicellulose, and ˜40 wt.% of cellulose. All the reagents were purchased from Sigma-Aldrich (SP-Brazil) ($NaClO_2$, 99 %, NaOH -95 %, KOH-98 %, ethanol–98 %).

2.2. Methods

2.2.1. Treatments

To obtain cellulose without the presence of lignin and hemicellulose, two chemical pre-treatments were carried out in sequence:

2.2.1.1. First treatment. The ES was first treated in a solution of $NaClO_2$ (3.8 wt.%) for 2 h at 50 °C under mechanical stirring, and then the obtained material was washed and dried in an oven at 50 °C for 12 h.

2.2.1.2. Second treatment. Subsequently, the material was treated in a solution of NaOH (10 wt.%) and KOH (10 wt.%) for 2 h under magnetic stirring, washed and dried at 50 °C for 12 h. After these treatments, the final material has in its composition ˜1.5 wt.% of hemicellulose and ˜2 wt.% of lignin, and this sample is named T_2. This methodology was previously reported [30]. The yield was ˜40 wt.%. Considering that the eucalyptus residues have ˜40 wt.% of cellulosic fibers and ˜60 wt.% of other non-cellulosic components, this yield is considered as excellent.

2.2.2. Isolation of nanocellulose

The treated sample, after the second treatment, was mixed with ethanol (80 % v/v) in the proportion 1:1 g/ml and subjected to 4 different milling times: 1 h, 2 h, 3 h, and 4 h, in a ball mill (MA500 - Marconi). This is rotational type mill, and the particles are shrunk by frictional and friction forces that occur between the balls, the jar wall, and the sample during the rotational movement of the jar. The speed of the milling is 200 rpm. The jars used are made of porcelain, model 21A (Chiarotti), with the following characteristics: diameter of 150 mm, height of 195 mm, capacity of 1 L. The jar had 70 % of its volume filled with balls and 30 % with samples. The jar was filled with 5 g of treated sample, 5 ml of ethanol, 305 g of larger alumina balls (diameter of 21 mm), and 44 g of smaller alumina balls (12 mm). The balls are 92 % pure, the other 8 % being silica or silicon dioxide. The ball mill conditions were selected according to our previous studies [20,31]. A photograph of the jar and balls used is presented in Fig. 1 S (Supplementary material). The production yield of the ball-milled product is ˜80 wt.% (this value was calculated comparing the sample added in the jar of ball mill and the sample obtained after the milling time).

After 1 h interval (each hour) of milling, the samples were oven-dried at 35 °C for 24 h to remove the ethanol. Then the samples in powder form were subjected to high-intensity ultrasonic treatment in a Sonics Vibra Cell, at the power of 400 W and 24 kHz, in a continuous process. During the ultrasonication, the samples were maintained under an ice bath. The tip diameter is 14 mm, with an amplitude of 20 %. For each sample, aqueous solutions containing 1 wt.% of NC were sonicated during the selected time: 10, 20, and 30 min. After the ultrasound, the samples were in suspension form (1 wt.%). The image presented in Fig. 1 represents the followed methodology in this study, and Table 1 shows the adopted nomenclatures.

2.2.3. Characterization

2.2.3.1. Fourier transform infrared spectroscopy. Fourier transform infrared spectroscopy (FT-IR) was conducted using a Frontier 94,942 (PerkinElmer, USA) in the range of 4000 to 400 cm^{-1} with 32 scans and a resolution of 4 cm^{-1} with attenuated total reflectance (ATR) accessory equipped with diamond. The FTIR relative crystallinity (index of crystallinity - IC) was calculated using the ratio of the absorption bands at 1369 and 1315 cm^{-1}, as reported by Lee et al. (2015) [32]. Pellet pressed samples were analyzed at room temperature.

2.2.3.2. Raman spectroscopy. All samples were analyzed with a Raman spectroscopy (XRD Raman Spectroscopy Thermo Scientific, Madison, USA). This system is equipped with a 780 nm wavelength with 5.0 mW power laser. Approximately 0.5 mm–1 mm length of each dried sample is analyzed at 50x magnification. The spectra were recorded, and each spectrum presented is an average of 3 different points on the sample. The data acquisition was carried out in a range of 100-3500 cm^{-1}, and 32 scans were accumulated in each sample with 4 cm^{-1} spectral resolution. All the graphs were baseline corrected (25 points) using OriginPro 2009. From the subtracted spectrum of the NCs, peak intensities for the 380 and 1096 cm^{-1} bands were measured. The intensity ratio I_{380}/I_{1096} was determined, and Raman crystallinity (index of crystallinity – IC) was calculated using Eq. 1 [32–34].

$$IC = \frac{[(I_{380} - I_{1096}) - 0.0286]}{0.0065} \quad (1)$$

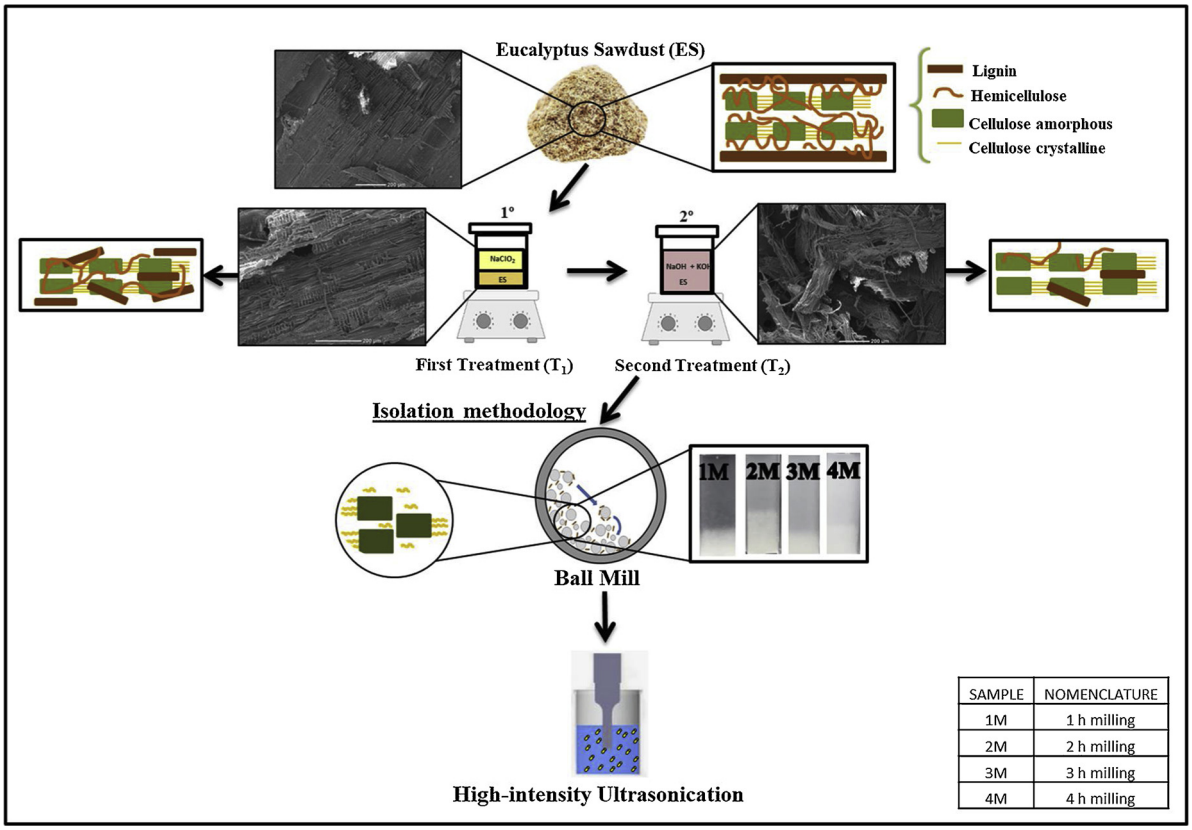

Fig. 1. Flow diagram representative of the preparation of nanocellulose: the pretreatment methods, followed by the mechanical grinding (ball mill) and finishing with assisted ultrasound methodology.

2.2.3.3. Dynamic and static light scattering. The isolated NC measurements were performed using dynamic light scattering (DLS) with a stable 90° scattering angle. Static light scattering (SLS) was conducted in the region 30–150 °. Both samples were performed using the ALV/CGS-3 instrument consisting of a polarized HeNe laser (22 mW). The equipment was operating at a wavelength (Ʌ) 633 nm, with NC diluted to a concentration of 0.01 wt%. The reading time established to obtain the DLS data was 10 s, and the measurements were performed in triplicate using the final average values. Hydrodynamic radius (R_H) was calculated by using Eq. 2 [35]:

$$R_H = \frac{K_B T}{3\pi\eta D} \quad (2)$$

Where: K_B is the Boltzmann's constant, T is the temperature, η is the viscosity, and D is the translational diffusion coefficient.

In the SLS experiment, the angular dependence of the absolute excess time-averaging (for a duration of scanning of 10 s) scattering intensity, known as the Rayleigh ratio R_{vv} (θ) leads to the mean square radius of gyration (R_G), which allows identification of the geometric shape of the objects (R_G/R_H) [36].

2.2.3.3.1. Morphological analysis – field emission scanning electron microscopy and transmission electron microscopy (FE-SEM and TEM). The surface morphology of all the samples was analyzed at different stages of treatments using FE-SEM (JEOL-JSM-7200 F) microscope equipped with energy-dispersive X-ray spectroscopy (EDS), with an acceleration voltage of 10 kV. The sample was prepared; drop of the NCs (2 wt.%) was dropped in the stub and after dried in the stove at 60 °C during 2 h. or Samples were mounted on carbon conductive tape and sputtered for around 5 min in Hummer 6.2 sputter system under 10 mA.

The microstructure and morphology of the samples with the best conditions were investigated by Transmission Electron Microscope (TEM-Joel 2010). A drop of the colloidal solution at 2 wt.% was deposited on a copper grid for analysis.

2.2.3.4. Zeta potential. The zeta potential measurement was determined using Zetasizer Nano-ZS (Malvern Instruments) to evaluate electrophoretic mobility of particles converted to Zeta potential using the Smoluchowski [30] Eq. 3. The reading time established to obtain the zeta potential data was 10 s, and the measurements were performed in triplicate using the final average

Table 1
Nomenclatures of samples prepared by varying milling and high-intensity ultrasonic times.

SAMPLE	NOMENCLATURE	SAMPLE	NOMENCLATURE
1 M	1 h milling	*3 M*	3 h milling
1 M-10U	1 h milling - 10 min ultrasound	*3 M-10U*	3 h milling - 10 min ultrasound
1 M-20U	1 h milling - 20 min ultrasound	*3 M-20U*	3 h milling - 20 min ultrasound
1 M-30U	1 h milling - 30 min ultrasound	*3 M-30U*	3 h milling - 30 min ultrasound
2 M	2 h milling	*4 M*	4 h milling
2 M-10U	2 h milling - 10 min ultrasound	*4 M-10U*	4 h milling - 10 min ultrasound
2 M-20U	2 h milling - 20 min ultrasound	*4 M-20U*	4 h milling - 20 min ultrasound
2 M-30U	2 h milling - 30 min ultrasound	*4 M-30U*	4 h milling - 30 min ultrasound

values. The NCs were diluted to a concentration of 0.01 % wt.%.

$$\zeta = \frac{3\eta U_E}{2\varepsilon f(ka)} \quad (3)$$

2.2.3.5. X-ray diffraction. X-ray powder diffraction data were collected on a D8 Focus diffractometer (Bruker AXS - Karlsruhe, Germany), operating at 40 kV and 40 mA, with monochromatic CuKα1 radiation (λ = 1.54056 Å) selected by a curved Ge (111) crystal monochromator. The data were collected from 10° to 60° in steps of 0.01° and a counting time of 100 s at each 0.5°. The index of crystallinity (IC) was calculated according to the following equation (Eq. (4)):

$$IC(\%) = (I_{200}\text{-}I_{am})/I_{200} * 100 \quad (4)$$

Where I_{200} is referred to the maximum intensity of the 200 lattice diffraction peak at 2θ = 22.2° and I_{am} is the intensity of diffraction for the amorphous part at 2θ = 18.5° [37,38].

2.2.3.6. X-ray photoelectron spectroscopy. The XPS analysis was conducted on a ThermoFisher Scientific, model K-alpha+, equipped with a monochromatic A1 Kα radiation at 1486.6 eV. The analysis was performed at room temperature and operated at 10 or 20 eV for high-resolution scans. Data were treated with CASAXPS software.

2.2.3.7. Thermogravimetric analysis. Thermogravimetric analysis (TGA) was carried out using STA 6000 instrument (PerkinElmer, USA). The samples were heated from 20 to 600 °C with a constant heating rate of 20 °C/min under nitrogen flow. All the graphs were analyzed using the software OriginPro 2009.

3. Results and discussion

3.1. Chemical characterization of the eucalyptus biomass and its nanocelluloses

A basic characterization of the chemical structure of the samples with different grinding and ultrasound times was conducted for a previous evaluation of the fiber composition and apparent crystallinity using FTIR and Raman spectroscopy. Fig. 2a presents the full spectra of the milled samples.

All the samples showed similar spectra, which is indicative of the similarity between the chemical composition of the samples [22]. It was observed bands of 3500-3200 and 2900 cm^{-1}, characteristic of the −OH binding and C–H symmetrical stretching groups of cellulose [31,39]. The bands around 898, 1030, 1160, 1315, 1369, and 1425 cm^{-1} were assigned to the C–H vibrations, C–O stretching, C–O-C asymmetric vibration, $-CH_2$ rocking vibration and $-CH_2$ deformation vibration of the cellulose, respectively [40].

Fig. 2a also shows a zoom of the region between 1800 and 1400 cm^{-1}; it is evident that all the milled samples do not show the peaks related to the lignin and hemicellulose [40,41]. Other peaks assigned to the cellulose structure are found at 1155, 1060, 1010, 990, and 893 cm^{-1}. Most of these peaks are influenced by neighboring bonds and their vibrational modes, which results in high band overlap and shift of some peaks, especially below 1100 cm^{-1}. After the milling, it was noted a significant decrease in the intensity of the band 1640 and 3400 − 3000 cm^{-1} due to the increase in the apparent crystallinity of the samples; increasing chain ordering, there is less available spacing for water entering the sample. Functional groups between 1300 to 800 cm^{-1} were observed; the increasing intensity of these groups indicates increased crystallinity of cellulose in the milled samples.

The apparent index of crystallinity (IC) was calculated for the samples 1 M, 2 M, 3 M, and 4 M. The sample ES showed an overlap of peaks due to the presence of non-cellulosic compounds, and it was not possible to calculate the "apparent" IC, as presented in Table 2 [16,32]. This value is not the real value and was used only for comparing the samples with each other [32].

The ball mill is a challenge composed of three main aspects: (i) energy and time, (ii) size and stability of nanoparticles, and (iii) wear: contamination and amorphization (Fig. 3).

In general, process optimization needs to balance the three challenges for shorter times and energy, smaller particle sizes, high stability, and crystallinity. According to the crystallinity values, it is not possible to unite all the desired characteristics in one material only with the ball mill: the sample 2 M showed high crystallinity (however, as presented in the next sections, the sizes were larger than the desire for this type of nanoparticles).

Less crystallinity of the cellulose obtained from samples 1 M, 3 M and 4 M are justified by the inefficient break resulting in the impact and shear forces or to the excessive time that resulted in the breaking of both the amorphous and crystalline regions. Combine mechanical method is an alternative to use low times in the ball mill and guarantee the aimed properties in the dimensional and stability characteristics of the nanocellulose.

The comparison between the FTIR spectra of the milled samples and its ultrasonicated samples is available in Fig. 2S on the supporting material. All samples showed slight increases in the IC since ultrasonic treatment acts in the separation of the nanoparticles. Longer times may have resulted in an entanglement of the fibers, which resulted in disturbance of the crystalline region. The FT-IR spectra analysis also allows a pre-selection of the samples based on the crystallinity: 2 h of milling and 20 min of ultrasonication.

Similar to observed in the FTIR analysis, Raman frequency, intensity, and band shape of the vibrations may vary between the nanocelluloses due to the differences in the chemical structure, interaction between the biopolymer chains, and its organization. In most cases, the peak sharpness and intensities are associated with the crystallinity of NC in which, increase in peak intensities increases in the crystallinity of NC as shown in Fig. 4a–b. Crystallinity percentage after ultrasonic irradiations drastically increase in all the study samples, as presented in Table 2; this may be due to the disruption of amorphous domains to yield nanocellulose because of ultrasonic irradiation.

Raman spectra of cellulose from eight different treatments were collected and compared to the literature data. Cellulose is a polysaccharide thus has characteristics Raman bands from 300 to 3000 cm^{-1}. The main cellulosic peaks are indicated with arrows, and corresponding peaks are ~380 and ~460 cm^{-1}: C—C—C, C–O, C—C–O ring deformation. The band at 900 cm^{-1} is associated with the C–H ring of cellulose and is the disorder of the cellulosic structure (amorphous region) [33]. Similarly, 1340 cm^{-1}: $-CH_2$, H—C—C, H—O—C—, and C–O—H; 1456 cm^{-1}: H—C and H—O—C bending. Raman bands from 1300 to 1500 cm^{-1} corresponding to $-CH_2$ and $-CH_2OH$ deformations are also reported [33]. The Raman bands at 2889 cm^{-1}: CH and CH_2 corresponding to stretching and bands at 3286 − 3402 cm^{-1}: O—H stretch [42].

Raman technique can result in estimate values of crystallinity, as presented in Fig. 4a–b. This value can be influenced by hemicelluloses (as impurities), and therefore other measurement methods need to be conducted and compared. of crystallinity by the ratio of cellulose's Raman bands at 380 and 1096 cm^{-1}. Also, the region of the sample or the preparation of the sample can influence the obtained values, and this is the reason why the results of crystallinity measurements by different researches have been, at times, contradictory [34].

It was possible to sequence the crystallinity for the milled samples as 2 M ~ 3 M > 1 M > 4 M; the results indicate that the best condition of milling time considering only the crystallinity of the samples is two hours. Evaluating the ultrasonicated samples, all of them showed significant increases in the crystallinity values. The defibrillation effect can justify the increase in the IC values after the high-intensity ultrasound: when the ultrasonic waves arrive at the sample, they penetrate the crystalline structure of the cellulose and result in the separation of

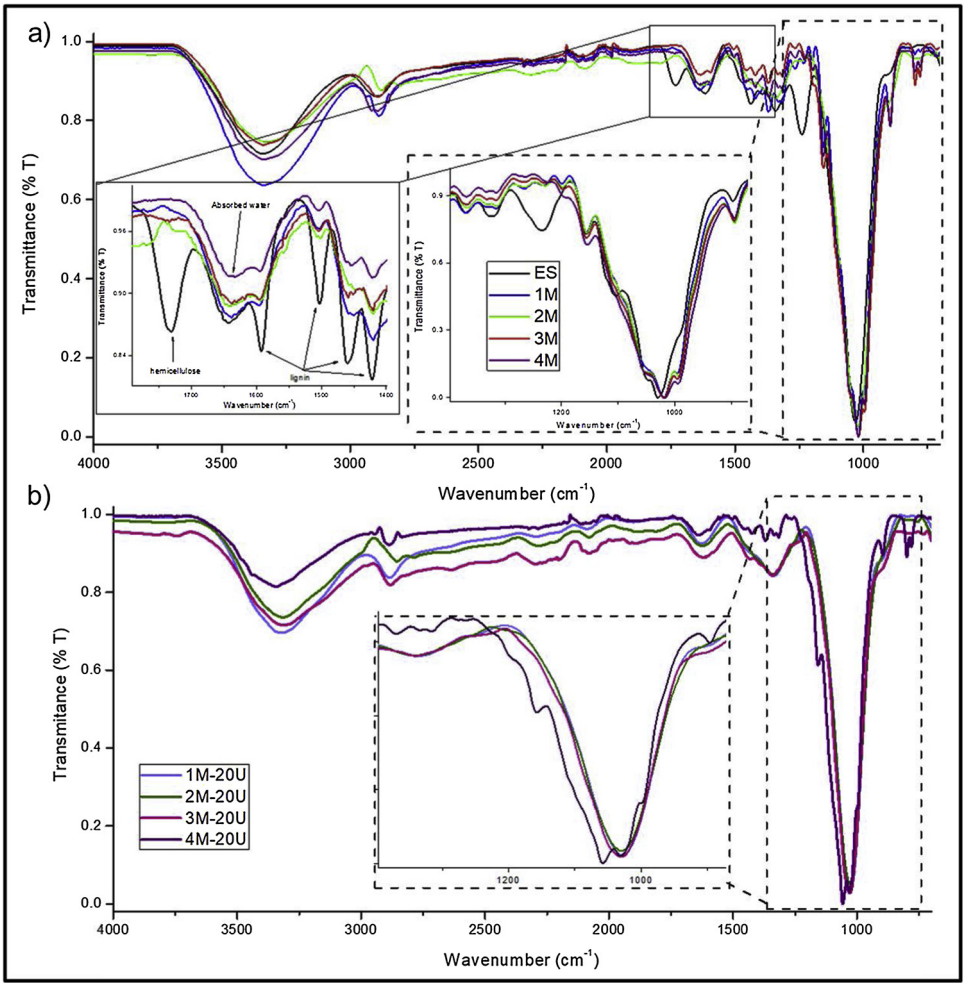

Fig. 2. Infrared spectra of (a) Eucalyptus (ES) and 1 M, 2 M, 3 M and 4 M samples and zoom in the region 1800 to 1400 cm^{-1} and 1390 to 600 cm^{-1}; and (b) full spectra for the ultrasound-20 min samples.

Table 2
Crystallinity values obtained from FTIR and Raman spectra.

Samples	Apparent IC (%) (FTIR) 1369/1315	Crystallinity (%) (Raman)
1 M	98.4	49.8
1 M-20U	99.3	57.9
2 M	99.4	59.9
2 M-20U	99.7	77.0
3 M	88.1	60.3
3 M-20U	89.9	73.5
4 M	98.1	17.7
4 M-20U	99.9	66.3

the nanofibrils. This separation, associated with the high shear force present in the solution, breaks the amorphous regions and isolates the crystalline ones, resulting in more separated and crystalline NCs. The more crystalline the sample ground, the easier the separation of nanofibrils, and therefore the best results among the ultrasonic samples are those for 2 h of milling.

3.2. Preliminary evaluation of sizes and shapes and morphological analysis

The milling was conducted in four different times: 1, 2, 3, and 4 h, and the effects of the different times were evaluated dimensionally. The DLS and SLS analysis allow a preliminary evaluation of the NC' sizes and shapes. The DLS measures the translational diffusion coefficient of particles in water, which undergo Brownian motion. The value given by this technique is the hydrodynamic radius (R_H) of a sphere having the same diffusion coefficient as the rod-like cellulose nanoparticles [8,43,44]. Fig. 3S shows the curves of the size distribution and information about the maximum, minimum, and average sizes of the milled samples.

Comparing the milled samples, in Fig. 3S, it was possible to observe that the $R_{H\ Average}$ was the lowest for 2 h of ball mill, followed for 3 h, 4 h, and 1 h. The milling time of the 1 h was not enough to break the fibers into nanostructures; the higher times (3 and 4 h) show a trend of increase de dimensions. The best milling time was 2 h. According to Sofla et al., longer grinding times may result in the growth of a fibrous layer of cellulose around the grinding balls. This fact decreases the impact power of the balls on the particles and results in larger sizes [45,46]. This behavior justifies the larger particle sizes of the samples 3 M and 4 M.

In all DLS measures, it was verified that the sample with 20 min of ultrasound showed the lowest R_H averages. Most of the particles also presented maximum sizes in the micrometric range is indicative of the more elongated morphology of the particles (nanofibrils – Fig. 6) [7,47]. This size trend can be observed in Fig. 5, which correlates the average particle size and ultrasound time.

Correlations with the SLS technique and morphological analyses were needed to confirm the shape of the NCs. In this way, SLS analysis was conducted, and Table 3 presents the obtained values of the hydrodynamic radius (*RH*), rotation radius (*RG*), distribution of sizes, and identification of the geometric shape of objects (RG/RH).

With the SLS data, it is possible to evaluate the parameter ρ, related

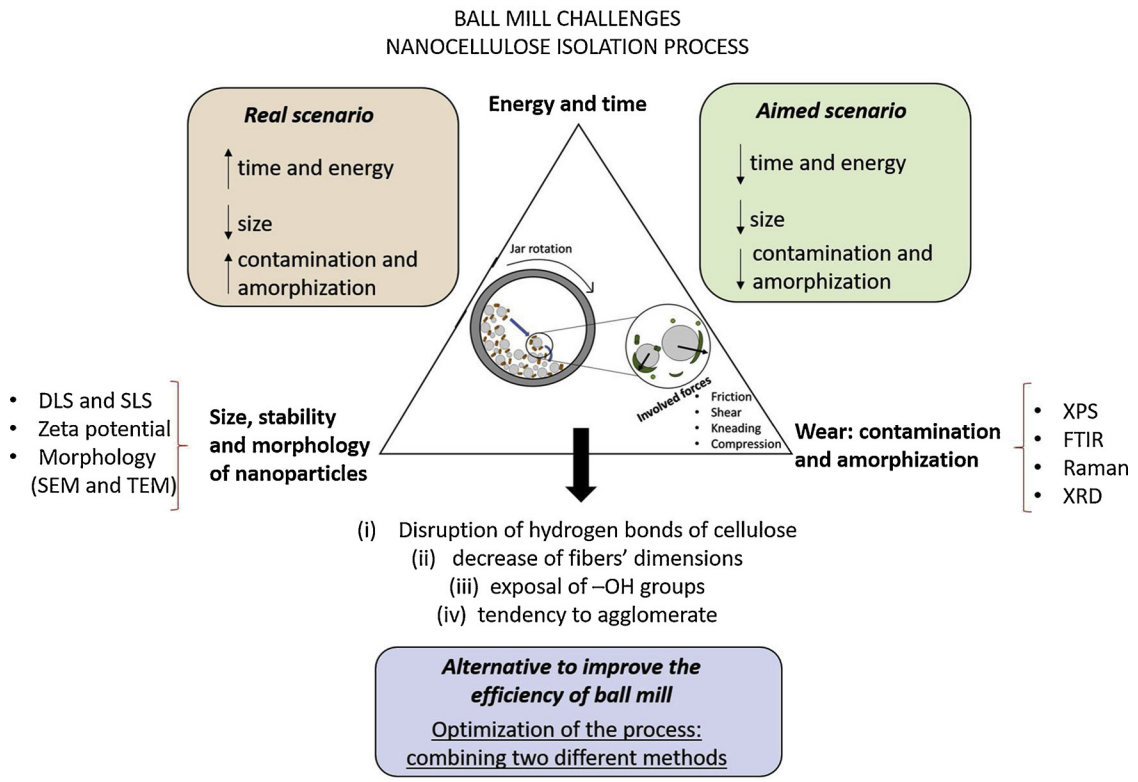

Fig. 3. Challenges of ball mill in the nanocellulose (NC) isolation, comparison between the real and the aimed scenario, and the main techniques that can be employed to analyze each NC characteristic.

to the R_G (obtained from SLS values) and R_H (obtained from DLS values). The R_G is a parameter defined as an average root mean squared distance from the center of the mass of a macromolecule. This parameter allows a correlation between the R_G/R_H and the morphology of the systems studied. It is a little-used technique for understanding cellulosic systems because of its complexity; however, it provides basic information in a short time.

According to Stetefeld et al., R_G/R_H ~1 can be attributed to elongated shapes [48]. It is possible to observe that there is much different information that needs to be compilated and corroborated with other morphological techniques. In the case of NCs, many shapes can occur, such as spheres, fibrils, and rod-like structures [31,49–51]. So, there is a limitation in the precise estimation of the shapes, resulting in approximate values.

According to the values, the time of 20 and 30-min ultrasound are considered adequate to obtain an elongated shape. The sample 1 M-30U ($\rho = 1.48$) and 2 M-20U ($\rho = 1.22$) are considered as an excellent morphology due to its ρ, which fits into the fibrillar morphology because they present the ratio of $\rho > 1$ [48].

To corroborate and complement the DLS and SLS results, the morphological analysis was conducted. Fig. 6a shows the FESEM images of the milled and ultrasonicated samples. The FESEM images validate the changes in the disintegration of the fibers, and the best samples were evaluated by TEM images, as shown in Fig. 6b that is the 2 h milled sample and 2 M assisted by 20 min of high-intensity ultrasound [70]. The best samples were determined according to the previous results presented in Fig. 4S.

The use of FESEM is limitated by the equipment conditions, being necessary to dry the samples, which results in agglomeration and overestimation of sizes. NC usually aggregate into bundles during the drying process, and that is why FESEM images are not so easy to see and individual nanoparticles could not be observed. Also, the surface of the

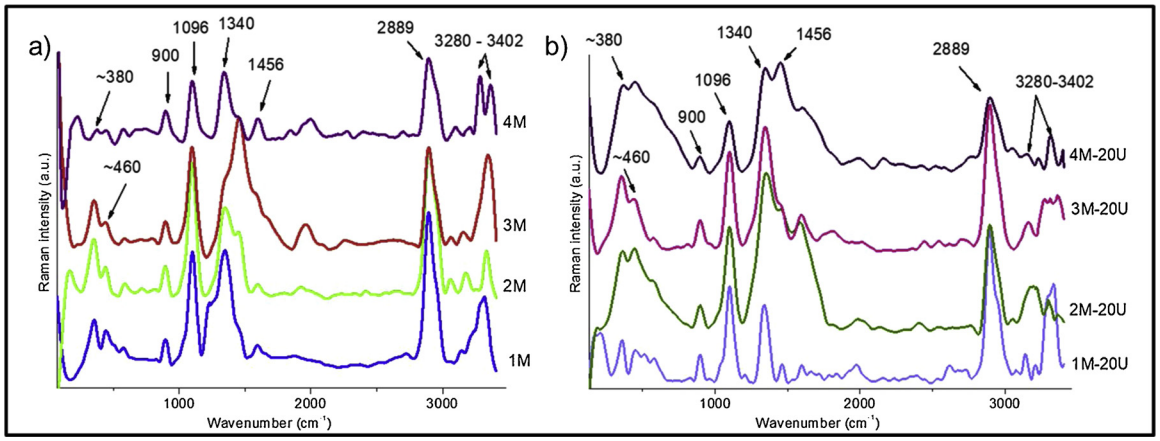

Fig. 4. Raman spectra of (c) milled and (d) ultrasonicated samples.

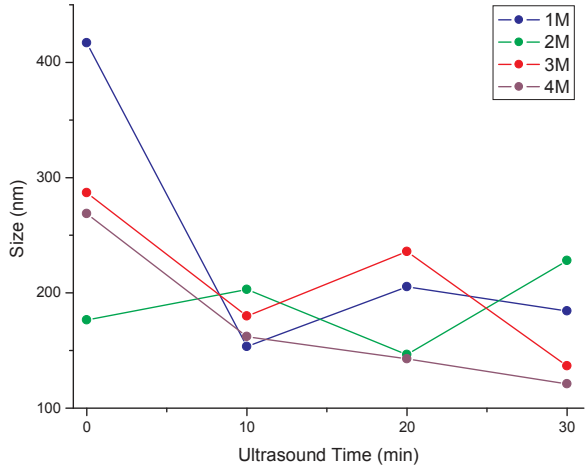

Fig. 5. Average hydrodynamic sizes of the NC vs. ultrasound time, measured by DLS analysis.

sample was coated with gold to obtain the images [71], and the coating broads the nanosized structure. However, this technique provided some interesting observations about the samples.

The use of the ball mill resulted in a non-uniform and random breaking of the cellulose fibers. Some fibers have better defibrillation, while others remain micrometric in size. In some FE-SEM images, it is possible to observe some regions have a quasi-circular shape, for example, in 4 M, 1 M-20U, 2 M-20U, and 4 M-20U. It is associated with the ball milling effect due to the breakage of the fibers along the direction perpendicular to the fiber axis [60].

Based on all other results observed during this work, it was concluded that the 2 M sample is the one with the most potential to obtain nanocellulose, and the use of 20 min of ultrasound was the time that presented the best results. In this way, the morphology verification using TEM was performed for these samples (Fig. 6b). It is interesting to observe that in sample 2 M, which was in solution and, therefore, in a dispersed state when compared to FESEM, presented diameters of approximately 400 − 600 nm and length of ˜5 µm, which result in an aspect ratio (L/D) of ˜8. After the ultrasound, these samples presented a drastic reduction of diameters, with an average value of ˜25 nm and length of ˜3 µm, which result in an aspect ratio (L/D) of ˜120 [71]. By these results, it is possible to conclude that the morphology of the obtained NCs are nanofibers.

In Fig. 6c is presented a scheme that represents the proposed explanation about the ultrasound effect on the NCs. The mechanical grinding by ball mill resulted in a random and irregular break due to the different forces that occur in the fibers: shear, friction, and compression. By using ultrasound as a combined method, ultrasound waves generate more defibrillation of fibers, which are already partially accessible, and these results are more visible with TEM images. It results in greater uniformity of sizes, smaller diameters, and more stability of the suspension.

3.3. Zeta potential

Zeta potential (δ) was measured to evaluate the electrostatic stability of the NCs, and the results are presented in Table 3. Values less than ± 15.0 mV represent the tendency to agglomeration and greater than ± 30.0 mV means that the samples show electrostatic charges [30,52,53]. The sample 1 M was the only that showed electrostatic instability, i.e., a tendency of aggregation and flocculation due to the low presence of free hydroxyl groups. It probably occurred due to the larger particle sizes, which mean lower surface area and lower availability of free hydroxyls; also, the gravitational forces act and tend to flocculate large particles. The other milled samples showed high δ values. Considering the δ values of the samples (Table 3), after the ultrasound, the samples 4 M reduced the stability of the suspension, for 3 M's there is no significant change in this properties, and the 2 M samples increased the stability for longer times of ultrasound, whereas the 1 M's the same behavior was observed. The sample 2 M-20U stood out with ˜60 mV, which means that there is possibly a greater availability of free hydroxyls that result in repulsive electrostatic charges [54,55]. The 2 h ball-milled, and 20-min ultrasound time was selected as the ideal time in this study, considering dimensional and surface characterization and the shortest time of use of ultrasound.

The suspensions were monitored as a function of time at 0, 10, and 30 min, as shown in Fig. 7. The milled samples show large particle sizes and aggregation tendency, being visible to the naked eye. After 10 min, the samples were deposited at the bottom of the container. The larger sizes and the superficial charges resulted in a high tendency to flocculation [56].

Samples that have passed through the ultrasound process showed better dispersibility. It is probably because the samples have smaller particle sizes since it is expected that the high-intensity ultrasonication promotes a good disintegration of the cellulose fibers. In this case, the high superficial area probably has high free hydroxyl contents, which contributes to the dispersibility of the suspension [57,58].

3.4. X-ray diffraction

The crystalline behavior of the milled samples before and after the high-ultrasonication was investigated using X-ray diffraction. Fig. 8a–b show the XRD patterns, and all the samples follow a similar trend exhibiting the principal crystal planes (200) and (004) at approximately 22.2 and 34.6°, respectively [22]. The small and broad peak at 34.5° represents the contribution of (040) plane. The index of crystallinity (IC) indicated that all the samples have a higher IC than the ES (raw); this could be justified with the removal of the non-cellulosic components (hemicellulose and lignin) after ultrasonic treatment [41]. Comparing with the IC calculated by FTIR analysis, it is possible to observe a similar trend, with the ultrasonicated samples but has a slight difference in the crystallinity values. This may occur because there may still be other lignocellulosic components present, and when used the FTIR technique, this may interfere significantly in the calculated values [32].

In Fig. 8a it is possible to observe that the samples presented IC values in the following order; 1 M > 4 M > 2 M > 3 M. The 1 M sample was subjected to less milling time resulting in fewer shocks and shear force. This demonstrates that despite reducing nanometer-scale particles, ball milling results in loss of crystallinity over time. One hypothesis for the 4 M sample to have been more crystalline than 2 M and 3 M is that there was enough breakdown of the cellulose crystalline region that was exposed and making this into the amorphous region.

The use of high-intensity ultrasound methodology presented results similar to those of grinding, as present in Fig. 8b. However, obtained NC with ultrasonically treated samples exhibited homogeneous dispersion and disintegration into individual particles due to the disruption of hydrogen bonds. Nevertheless, some authors mentioned the limitations of this method, mainly due to the underestimation of the contribution of the amorphous region, overestimating the IC [41]. One justification for the similarity between the IC values is that no acid was used for the dissolution of the amorphous region, only breakage. As the NC solutions do not undergo any washing, as reported in the experimental part, there is no separation between amorphous and crystalline regions. For a better understanding of the difference between methods, the morphological analysis was used. Similar results were reported by Chen et al. [59,60].

Based on the previous results of crystallinity and nanosizes, these parameters were evaluated to determine the most favorable condition to obtain NC. The compilated results are presented in Fig. 4S, in the Supplementary Material, and show that the 2 h of milling (sample 2 M) was considered the ideal grinding time. Also, concerning the ultrasound

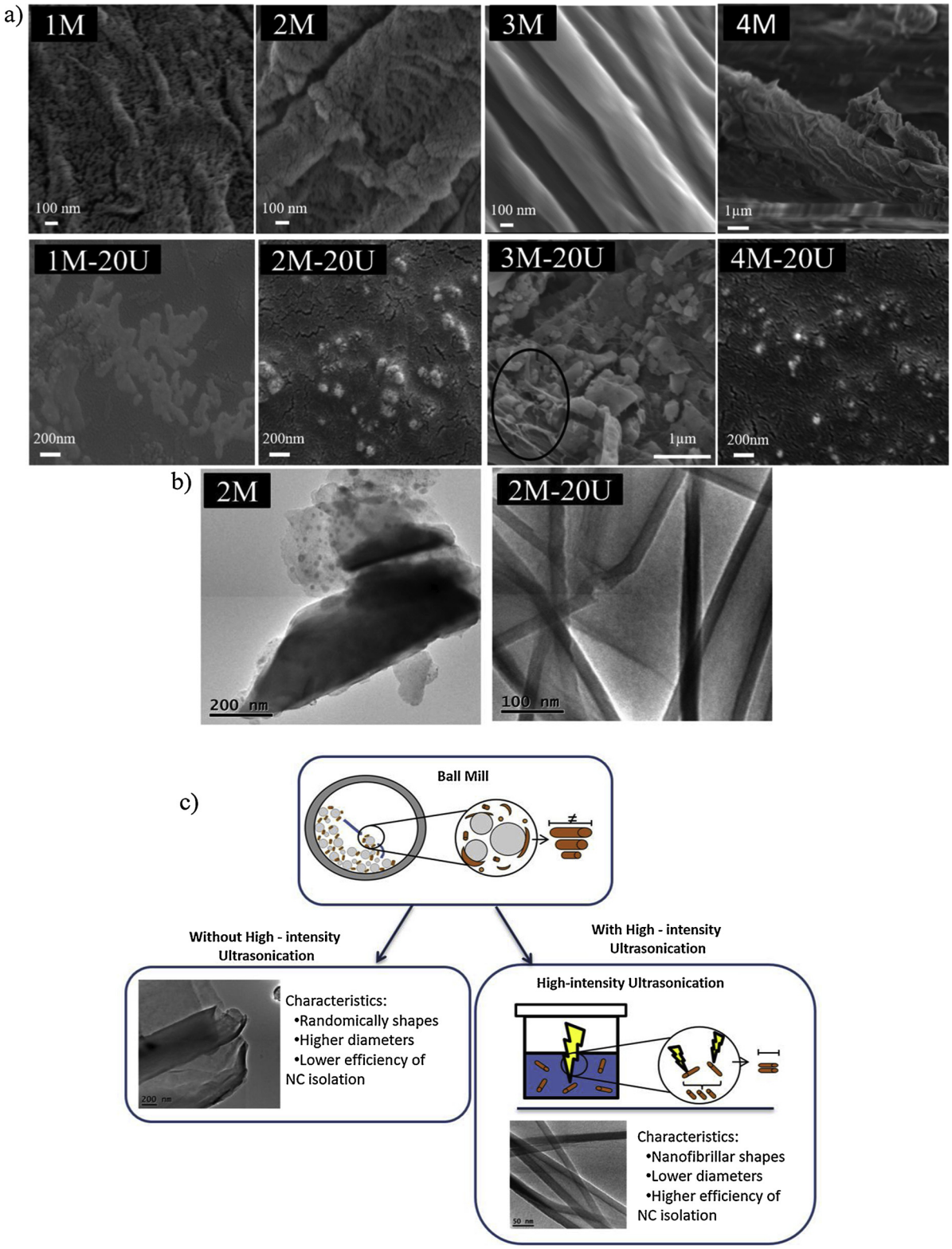

Fig. 6. (a) FESEM images of the milled and ultrasonicate samples and (b) TEM micrographs of the best conditions: 2 M and 2 M-20U; (c) Scheme shows the main consideration about the effect of the high-intensity ultrasonic.

times evaluated, the use of 20 min presented more uniform sizes and smaller size distribution. Thus, the most effective combination of methods was for 2 h of milling assisted with 20 min of ultrasound.

3.5. Evaluation of the composition and eventual contamination of the NCs

The high-resolution XPS spectra were collected for the milled samples and the ultrasonicated samples for 20 min (Fig. 8c–d), respectively. It was observed that increasing the milling time there is the presence of Al and Si. These elements are impurities associated with the

Table 3
Structural parameters using light scattering techniques (RH values were obtained from DLS and RG values from SLS), and zeta potential values.

Samples	R_H (nm)	R_G (nm)	ρ (R_G/R_H)	Zeta potential (mV)
1 M	2840.0	338.3	0.12	−24.7
1 M-10U	453.6	132.6	0.29	−51.7
1 M-20U	361.4	156.6	0.43	−40.8
1 M-30U	113.4	167.3	1.48	−40.9
2 M	246.8	221.4	0.90	−43.5
2 M-10U	450.9	173.5	0.39	−42.1
2 M-20U	145.9	177.3	1.22	−59.3
2 M-30U	826.0	150.8	0.18	−53.5
3 M	2600.0	306.8	0.19	−45.0
3 M-10U	544.6	197.5	0.36	−45.7
3 M-20U	488.8	156.1	0.32	−39.3
3 M-30U	277.6	167.7	0.60	−45.7
4 M	240.1	207.3	0.86	−45.7
4 M-10U	301.4	131.1	0.44	−48.1
4 M-20U	374.5	143.4	0.38	−40.7
4 M-30U	216.8	154.3	0.71	−40.5

jar and balls composition (SiO_2 and alumina), and higher times of milling resulted in higher contents of impurities. The O/C ratio was calculated, and the obtained values are 0.39, 0.49, 0.54, 0.68, and 0.75 for the samples ES, 1 M, 2 M, 3 M, and 4 M, respectively. The theoretical value of pure cellulose is 0.83 [61].

Alumina is the main composition of the jar and spheres; Silicon dioxide is the "contaminant" mostly found in the balls. Interestingly, as milling time increased, the aluminum concentration was constant and low; however, there was an increase in silicon content due to the wear of the balls, which mainly occurs in the region of impurities, resulting in contamination of the cellulose. The use of other materials as grinding agents such as high alumina or zirconic spheres could significantly reduce contamination but would result in an increase of approximately 20 % in cost.

For the ultrasonicated samples, the values are 0.61, 0.64, 0.61, and 0.79 for the samples 1 M-20U, 2 M-20U, 3 M-20U, and 4 M-20U, respectively. The ultrasound samples showed higher O/C values than the milled samples. This difference in NC values is due to the chemical pretreatment and the combinatorial isolation method used to obtain NCs from the ES fibers, in which the ball mill allowed the partial removal of oxygen from the NCs while the high-intensity ultrasound caused a closer increase of pure NC (0.83), as reported in the literature [62].

3.6. Thermogravimetric analysis (TGA)

The thermal analysis gives information about the thermal behavior of the ES and NC derived from it as well as possible high-temperatures applications of NC [22]. The results obtained by the thermogravimetric analysis were plotted as thermogravimetric and its derivative curves, as in Fig. 9a–b.

The TGA curves maintained a similar pattern for all the samples, which is in agreement with the conventional curves of NC [53,63–68].

All these samples showed two main events of percentage weight loss. The first is related to the breakage of inter- and intramolecular hydrogen bonds corresponding to water evaporation [30,58]. The second event of weight loss is related to the thermal degradation of cellulose. The ES sample had slightly higher thermal degradation temperatures than the NCs. Nanoparticles have larger surface areas than ES, which may have catalyzed thermal degradation. All the milled samples showed very similar T_{max}, even at high mechanical milling times, which indicates that all the structures are identical, and similar energies are required to thermal degradation of the cellulose.

There was an increase in decomposition temperature by 10 °C in all the ultrasonically treated samples than ball-milled samples. This small change could be due to the more ordered and individualized structures which corroborate with the previously presented crystallinity results. Another possibility is that the surface area of the NC is very high, which means that the heat can be disseminated very quick, and it can decrease the thermal decomposition temperature of the samples.

This behavior is another indication of the efficiency of the combined methods since the high temperatures are justified by the higher energy necessary for the thermal degradation of the nanocelluloses [69]. These results are promising and demonstrate that the combination of the two insulation methods may favor applications that require higher

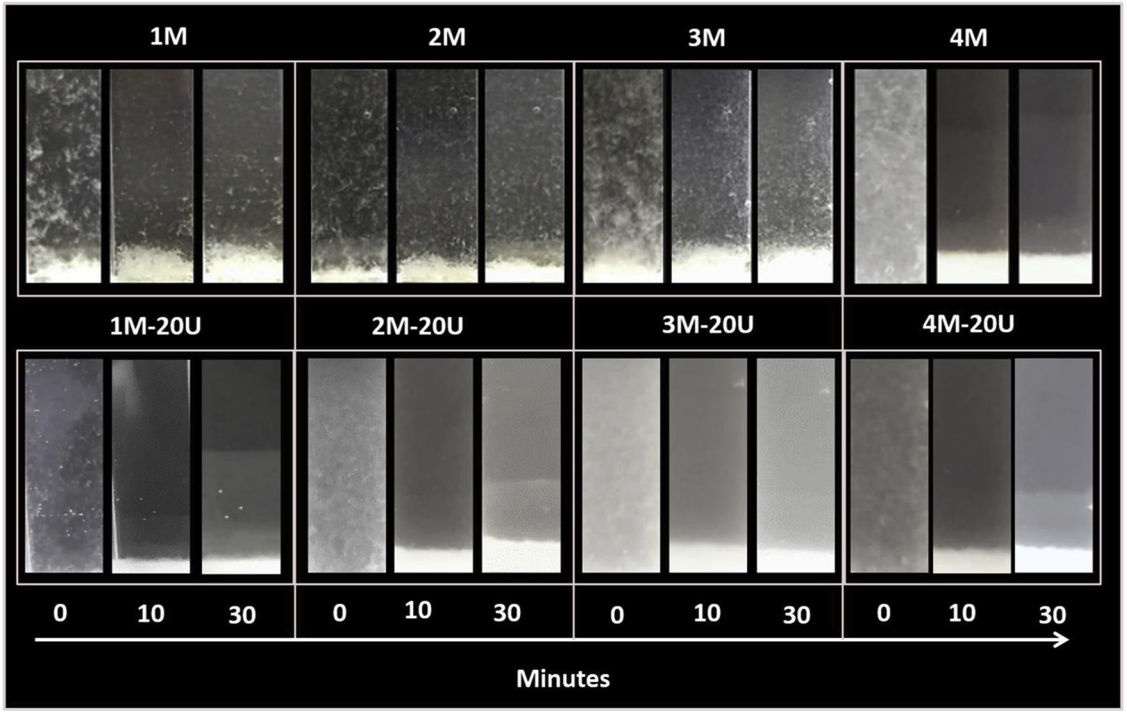

Fig. 7. Samples suspensions at the times of 0, 10, and 30 min.

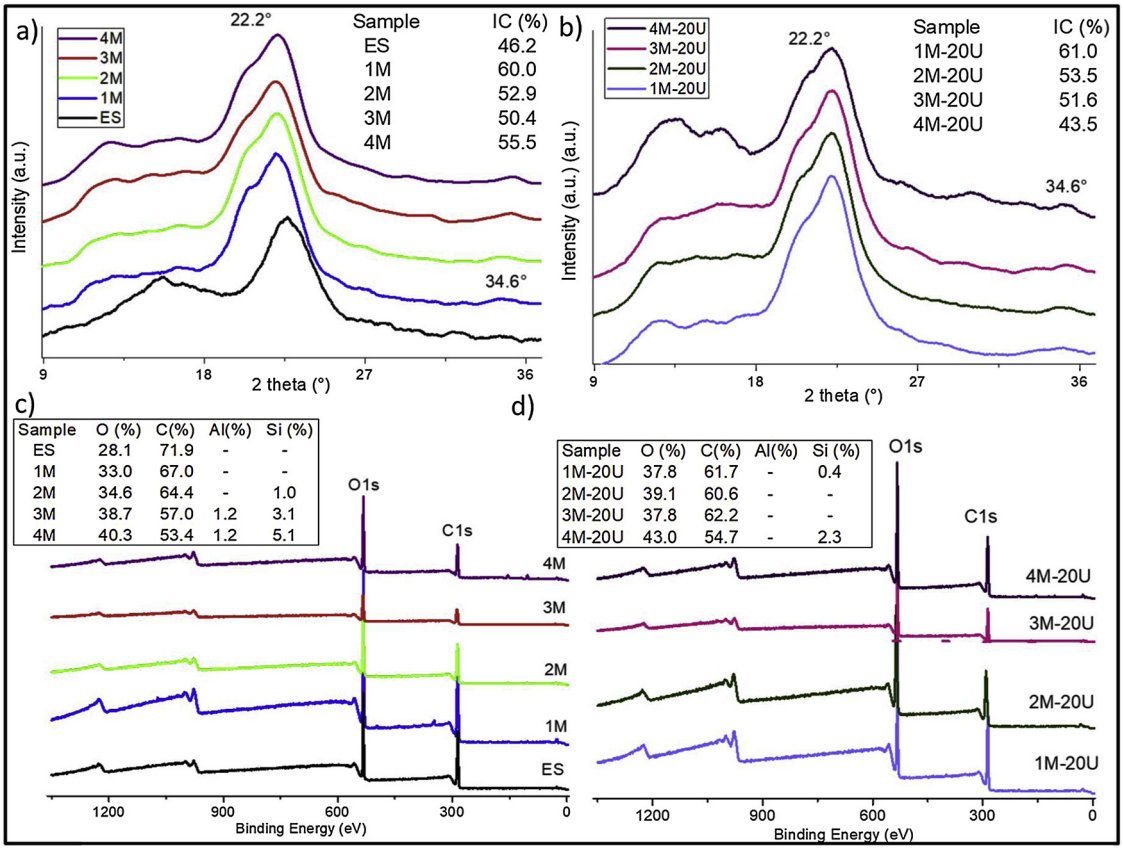

Fig. 8. X-ray diffraction patterns of (a) milled samples and (b) ultrasonicated samples; XPS survey spectra (0–1400 eV) for (c) eucalyptus sawdust and milled NCs and (d) ultrasonicated samples, showing the representative C 1s (286 eV) and O 1s (532 eV) photoemission peaks.

processing temperatures.

3.7. Final remarks

Nanocellulose, with exceptional intrinsic properties such as excellent thermal and dimensional stability, crystallinity, and stiffness, has been prominent in the world bioeconomy as a potential substitute for carbon and graphene nanotubes. This is because this material has high added value and is a class of compatible and renewable bionanomaterials. This reflects a worldwide race for NC production with high productivity, process efficiency, and low environmental impacts. Considering industrial production or pilot-scale, some companies may be cited. VTT Finland is developing a project to obtain NC with enzymatic processes; Paperlogic has a production capacity of 2 tons per day; Fibria Insights is already investing in innovative projects to develop viable processes for obtaining NCs; In addition, numerous start-ups are springing up around the world to develop these high-quality, high-quality advanced materials [29,72–74].

It should be noted, however, that many companies, in addition to targeting high-capacity production processes, have also shown a keen interest in developing more environmentally friendly techniques [75]. Although numerous researches are being conducted, there is still a limitation on mechanical methods due to commonly used equipment. Thus, the combinatorial approach presented in this work stands out for using common equipment in other industrial areas (such as paints and ceramic suspensions), without using toxic reagents. There is a clear and growing trend in the development of methods and processes aimed at lowering prices and increasing nanocellulose productivity, which has proven to be a "material of the future".

4. Conclusions

Nanocellulose (NC) was successfully isolated from eucalyptus sawdust using a combination of ball mill and high-intensity ultrasonication methods; all the proposed milling times (1, 2, 3, and 4 h) resulted in cellulosic particles in the nanometric scale. The use of a combinatorial method to overcome the challenges encountered in mechanical grinding without the use of chemical reagents was successful; the ultrasound

allows defibrillation of the nanofibres by reducing NC diameters, as well as providing high power output, concentrated energy transfer, low cost and ecological character. The 2 h-milling times presented smaller size, following by 3 M < 4 M < 1 M. After the milling, the ultrasound irradiation was conducted in 10, 20, and 30 min. The 20 min samples showed the smaller sizes and high electrostatic stability when compared to the other evaluated times; and according to static light scattering, this sample has random morphology with elongated form, which is desired for NC.

The crystallinity values (CI), determined by FTIR, Raman, and XRD, show a similar trend. The 2 h-milled sample presented a high crystallinity, and the CI values followed the order 2 h˜3 h > 4 h > 1 h; longer times (4 h) may have a disturbance in the crystalline region; low times (1 h) was not enough to break and remove the amorphous region. Also, the use of ultrasound increased the thermal stability, which can be justified by the increase in the crystallinity of the samples.

It was verified that the mechanical grinding results in a random and irregular break of the cellulose fibers due to the shear and friction forces. So, in the combined method, the ultrasound waves generate more defibrillation of nanofibers, decreasing the NC' diameters. Short ultrasonic times are not enough for the separation of the nanofibers, whereas excessive times induce a disorder and entanglement of the NC. Also, they produce fibers with fewer contaminants, according to XPS

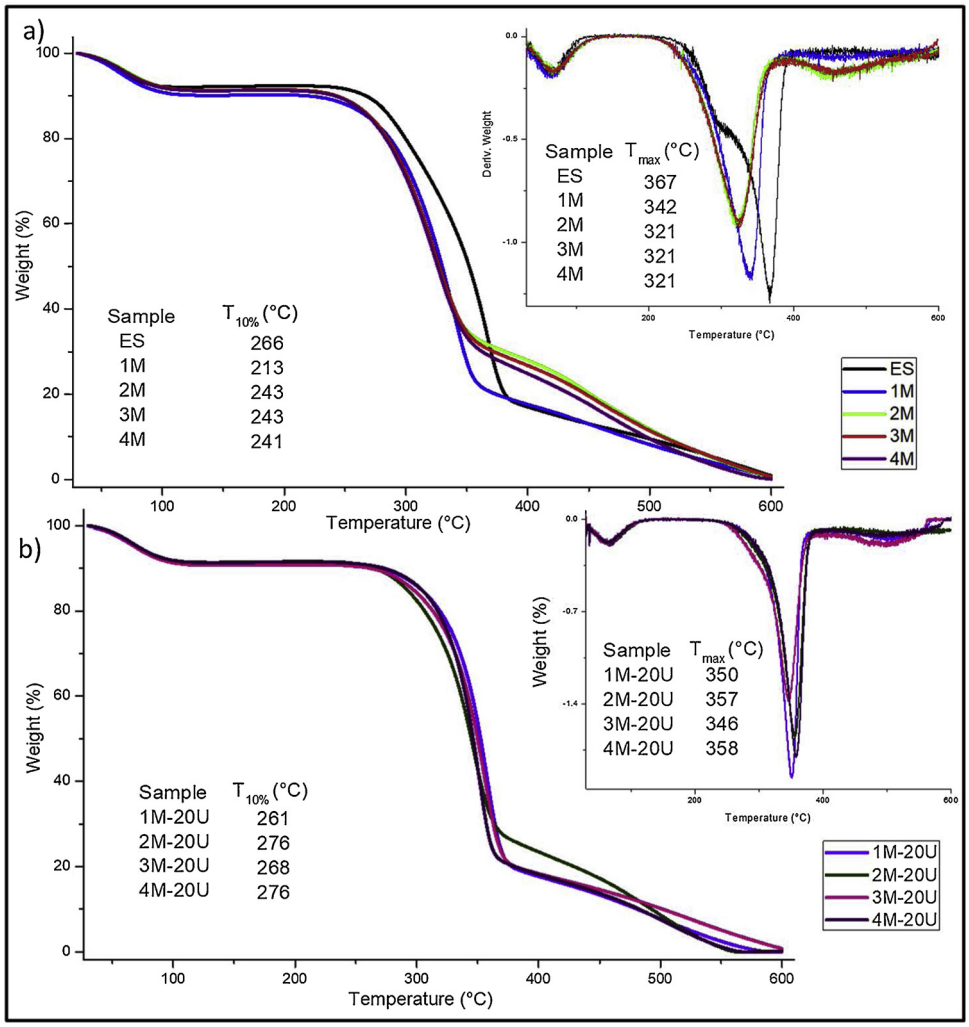

Fig. 9. Thermal behavior of the ES sample and their prepared nanoparticles. ES and their nanocelluloses thermograms without (a) and with (b) the use of ultrasound. The inserts are the corresponding DTG curves.

results.

This study allowed an in-depth understanding of the combining method of grinding and ultrasound, which is a completely toxic-free and widely applicable method. The presented results suggest that the proposed method has a high potential and alternative way to unravel highly dispersive NC from natural resources. Also, the obtained nanoparticles are expected to show high potential as nanocellulosic reinforcement into a polymeric matrix, providing value-added materials with superior performance and biodegradable character. The applications are innumerous, such as agricultural plastics, packaging, oil emulsification, and others.

Declaration of Competing Interest

The authors declare that there are no conflicts of interest.

Acknowledgments

The authors thank the financial support provided by FAPESP (2018/11277-7 and 2018/25239-0), CNPq (305819/2017-8), CAPES (Code 001), NSF-CREST #1735971, and the Multiuser Experimental Center of the Federal University of ABC (CEM-UFABC).

Appendix A. Supplementary data

Supplementary material related to this article can be found, in the online version, at doi: https://doi.org/10.1016/j.mtcomm.2019.100755.

References

[1] C.L. Pirich, G.F. Picheth, J.P.E. Machado, C.N. Sakakibara, A.A. Martin, R.A. de Freitas, M.R. Sierakowski, Influence of mechanical pretreatment to isolate cellulose nanocrystals by sulfuric acid hydrolysis, Int. J. Biol. Macromol. 130 (2019) 622–626, https://doi.org/10.1016/j.ijbiomac.2019.02.166.
[2] F. and agriculture organization of the U.N. FAO, Global data on forest plantations resources, (n.d.). http://www.fao.org/3/Y2316E/y2316e0b.htm.
[3] J.O. Brito, F.G. Silva, M.M. Leão, G. Almeida, Chemical composition changes in eucalyptus and pinus woods submitted to heat treatment, Bioresour. Technol. 99 (2008) 8545–8548, https://doi.org/10.1016/j.biortech.2008.03.069.
[4] P. Indu, Dados Estatísticos, (2013), pp. 1–3.
[5] P. Phanthong, G. Guan, Y. Ma, X. Hao, A. Abudula, Effect of ball milling on the production of nanocellulose using mild acid hydrolysis method, J. Taiwan Inst. Chem. Eng. 60 (2016) 617–622, https://doi.org/10.1016/j.jtice.2015.11.001.
[6] R. da Silva, M.A. Woehl, C.N. Sakakibara, A.A. Martin, M.R. Sierakowski, G.F. Picheth, C.L. Pirich, C.F. de Souza, R.A. de Freitas, Bacterial cellulose in biomedical applications: a review, Int. J. Biol. Macromol. 104 (2017) 97–106, https://doi.org/10.1016/j.ijbiomac.2017.05.171.
[7] T. Kos, A. Anžlovar, M. Kunaver, M. Huskić, E. Žagar, Fast preparation of nanocrystalline cellulose by microwave-assisted hydrolysis, Cellulose 21 (2014) 2579–2585, https://doi.org/10.1007/s10570-014-0315-2.
[8] M. Kunaver, A. Anžlovar, E. Žagar, The fast and effective isolation of nanocellulose from selected cellulosic feedstocks, Carbohydr. Polym. 148 (2016) 251–258,

https://doi.org/10.1016/j.carbpol.2016.04.076.
[9] S. Bee, A. Hamid, H.Vc. of L.B. to N.: S. and C.P.C. Lee, S.B. a Hamid, S.K. Zain, rsion of Lignocellulosic Biomass to Nanocellulose :, 2014 (2015). doi:10.1155/2014/631013.
[10] A.G. de Souza, D.B. Rocha, F.S. Kano, D.dosS. Rosa, Valorization of industrial paper waste by isolating cellulose nanostructures with different pretreatment methods, Resour. Conserv. Recycl. 143 (2019) 133–142, https://doi.org/10.1016/j.resconrec.2018.12.031.
[11] W. Pan, X. Zhang, F. Niu, M. Li, J. Li, J. Yang, Q. Huang, The characteristic and dispersion stability of nanocellulose produced by mixed acid hydrolysis and ultrasonic assistance, Carbohydr. Polym. 165 (2017) 197–204, https://doi.org/10.1016/j.carbpol.2017.02.048.
[12] Z. Karim, S. Afrin, Q. Husain, R. Danish, Necessity of enzymatic hydrolysis for production and functionalization of nanocelluloses, Crit. Rev. Biotechnol. 37 (2017) 355–370, https://doi.org/10.3109/07388551.2016.1163322.
[13] C.J. Garvey, P. Memmott, P.K. Annamalai, D.J. Martin, E. Jiang, N. Amiralian, High aspect ratio nanocellulose from an extremophile spinifex grass by controlled acid hydrolysis, Cellulose 24 (2017) 3753–3766, https://doi.org/10.1007/s10570-017-1379-6.
[14] T. Theivasanthi, F.L. Anne Christma, A.J. Toyin, S.C.B. Gopinath, R. Ravichandran, Synthesis and characterization of cotton fiber-based nanocellulose, Int. J. Biol. Macromol. 109 (2018) 832–836, https://doi.org/10.1016/j.ijbiomac.2017.11.054.
[15] J. Hu, D. Tian, S. Renneckar, J.N. Saddler, Enzyme mediated nanofibrillation of cellulose by the synergistic actions of an endoglucanase, lytic polysaccharide monooxygenase (LPMO) and xylanase, Sci. Rep. 8 (2018) 1–15, https://doi.org/10.1038/s41598-018-21016-6.
[16] N. Kruer-Zerhusen, B. Cantero-Tubilla, D.B. Wilson, Characterization of cellulose crystallinity after enzymatic treatment using Fourier transform infrared spectroscopy (FTIR), Cellulose 25 (2018) 37–48, https://doi.org/10.1007/s10570-017-1542-0.
[17] M. Nuruddin, M. Hosur, M. Jamal Uddin, D. Baah, S. Jeelani, A novel approach for extracting cellulose nanofibers from lignocellulosic biomass by ball milling combined with chemical treatment, J. Appl. Polym. Sci. 133 (2016), https://doi.org/10.1002/app.42990.
[18] M.C. Guimara, Evaluation of the Effect of Processing Conditions on the Impact Properties of, (2017), https://doi.org/10.1177/0021998316688338.
[19] S. Mondal, Preparation, properties and applications of nanocellulosic materials, Carbohydr. Polym. 163 (2017) 301–316, https://doi.org/10.1016/j.carbpol.2016.12.050.
[20] F.S. Kano, A.G. de Souza, D.dosS. Rosa, Variation of the milling conditions in the obtaining of nanocellulose from the paper sludge, Matéria (Rio Janeiro). 24 (2019), https://doi.org/10.1590/s1517-707620190003.0719.
[21] C.C. Piras, S. Fernández-Prieto, W.M. De Borggraeve, Ball milling: a green technology for the preparation and functionalisation of nanocellulose derivatives, Nanoscale Adv. 1 (2019) 937–947, https://doi.org/10.1039/c8na00238j.
[22] C.M.E. Xuran, L. Min, W.Y. Huang, C.M. Ewulonu, Á.X. Liu, Á.M. Wu, Á.Y. Huang, X. Liu, Ultrasound-assisted mild sulphuric acid ball milling preparation of lignocellulose nanofibers (LCNFs) from sunflower stalks (SFS), Cellulose 4 (2019), https://doi.org/10.1007/s10570-019-02382-4.
[23] Z. Ling, T. Wang, M. Makarem, M. Santiago Cintrón, H.N. Cheng, X. Kang, M. Bacher, A. Potthast, T. Rosenau, H. King, C.D. Delhom, S. Nam, J. Vincent Edwards, S.H. Kim, F. Xu, A.D. French, Effects of ball milling on the structure of cotton cellulose, Cellulose 26 (2019) 305–328, https://doi.org/10.1007/s10570-018-02230-x.
[24] Y. Zheng, Z. Fu, D. Li, M. Wu, Effects of ball milling processes on the microstructure and rheological properties of microcrystalline cellulose as a sustainable polymer additive, Materials (Basel) 11 (2018) 1–13, https://doi.org/10.3390/ma11071057.
[25] H.P.S. Abdul Khalil, Y. Davoudpour, M.N. Islam, A. Mustapha, K. Sudesh, R. Dungani, M. Jawaid, Production and modification of nanofibrillated cellulose using various mechanical processes: a review, Carbohydr. Polym. 99 (2014) 649–665, https://doi.org/10.1016/j.carbpol.2013.08.069.
[26] A. Barakat, C. Mayer-Laigle, A. Solhy, R.A.D. Arancon, H. De Vries, R. Luque, Mechanical pretreatments of lignocellulosic biomass: towards facile and environmentally sound technologies for biofuels production, RSC Adv. 4 (2014) 48109–48127, https://doi.org/10.1039/c4ra07568d.
[27] R.J. Moon, A. Martini, J. Nairn, J. Simonsen, J. Youngblood, Cellulose Nanomaterials Review: Structure, Properties and Nanocomposites, (2011), https://doi.org/10.1039/c0cs00108b.
[28] J. Desmaisons, E. Boutonnet, M. Rueff, A. Dufresne, J. Bras, A new quality index for benchmarking of different cellulose nanofibrils, Carbohydr. Polym. 174 (2017) 318–329, https://doi.org/10.1016/j.carbpol.2017.06.032.
[29] M.S. Reid, M. Villalobos, E.D. Cranston, Benchmarking cellulose nanocrystals: from the laboratory to industrial production, Langmuir 33 (2017) 1583–1598, https://doi.org/10.1021/acs.langmuir.6b03765.
[30] G.F. de Lima, A.G. de Souza, D.S. Rosa, Effect of adsorption of polyethylene glycol (PEG), in aqueous media, to improve cellulose nanostructures stability, J. Mol. Liq. 268 (2018) 415–424, https://doi.org/10.1016/j.molliq.2018.07.080.
[31] A.G. De Souza, F.S. Kano, J.J. Bonvent, D.S. Rosa, Cellulose Nanostructures Obtained From Waste Paper Industry : A Comparison of Acid and Mechanical Isolation Methods, (2017), pp. 1–6.
[32] C. Lee, K. Dazen, K. Kafle, A. Moore, D.K. Kohnson, S. Park, S.H. Kim, Correlations of Apparent Cellulose Crystallinity Determined by XRD, NMR, IR, Raman, and SFG Methods, in: Adv. Polym. Sci. Springer International Publishing, Switzerland, 2015, pp. 1–34, https://doi.org/10.1007/12.
[33] U.P. Agarwal, Raman spectroscopy in the analysis of cellulose nanomaterials, Nanocelluloses Their Prep. Prop. Appl. ACS Sympos (2017) 75–90, https://doi.org/10.1021/bk-2017-1251.ch004.
[34] U.P. Agarwal, Raman Spectroscopy of CNC- and CNF-based nanocomposites, Handb. Nanocellulose Cellul. Nanocompos. (2017) 609–625, https://doi.org/10.1002/9783527689972.ch18.
[35] A. Jäger, E. Jäger, F. Surman, A. Höcherl, B. Angelov, K. Ulbrich, M. Drechsler, V.M. Garamus, C. Rodriguez-Emmenegger, F. Nallet, P. Štěpánek, Nanoparticles of the poly([N-(2-hydroxypropyl)]methacrylamide)-b-poly[2-(diisopropylamino)ethyl methacrylate] diblock copolymer for pH-triggered release of paclitaxel, Polym. Chem. 6 (2015) 4946–4954, https://doi.org/10.1039/c5py00567a.
[36] H.L. Yi, L.J. Lai, J.S. Jiang, C.C. Hua, Ethylcellulose colloids incubated in dilute solution, J. Phys. Chem. B 121 (2017) 638–648, https://doi.org/10.1021/acs.jpcb.6b09976.
[37] S. Nam, A.D. French, B.D. Condon, M. Concha, Segal crystallinity index revisited by the simulation of X-ray diffraction patterns of cotton cellulose Iβ and cellulose II, Carbohydr. Polym. 135 (2016) 1–9, https://doi.org/10.1016/j.carbpol.2015.08.035.
[38] L. Segal, J.J. Creely, A.E. Martin, C.M. Conrad, An empirical method for estimating the degree of crystallinity of native cellulose using the X-ray diffractometer, Text. Res. J. 29 (1959) 786–794, https://doi.org/10.1177/004051755902901003.
[39] R.M. de Sá, C.S. de Miranda, N.M. José, Preparation and characterization of nanowhiskers cellulose from fiber arrowroot (Maranta arundinacea), Mater. Res. 18 (2015) 225–229, https://doi.org/10.1590/1516-1439.366214.
[40] R.A. Ilyas, S.M. Sapuan, M.R. Ishak, Isolation and characterization of nanocrystalline cellulose from sugar palm fibres (Arenga Pinnata), Carbohydr. Polym. (2017), https://doi.org/10.1016/j.carbpol.2017.11.045.
[41] F. Kallel, F. Bettaieb, R. Khiari, A. García, J. Bras, S.E. Chaabouni, Isolation and structural characterization of cellulose nanocrystals extracted from garlic straw residues, Ind. Crops Prod. 87 (2016) 287–296, https://doi.org/10.1016/j.indcrop.2016.04.060.
[42] J.S. Lupoi, E. Gjersing, M.F. Davis, Evaluating lignocellulosic biomass, its derivatives, and downstream products with Raman spectroscopy, Front. Bioeng. Biotechnol. 3 (2015) 1–18, https://doi.org/10.3389/fbioe.2015.00050.
[43] Y. Boluk, C. Danumah, Analysis of cellulose nanocrystal rod lengths by dynamic light scattering and electron microscopy, J. Nanopart. Res. 16 (2014), https://doi.org/10.1007/s11051-013-2174-4.
[44] Y. Mao, K. Liu, C. Zhan, L. Geng, B. Chu, B.S. Hsiao, Characterization of nanocellulose using small-angle neutron, X-ray, and dynamic light scattering techniques, J. Phys. Chem. B 121 (2017) 1340–1351, https://doi.org/10.1021/acs.jpcb.6b11425.
[45] V.K. Baheti, R. Abbasi, J. Militky, Ball milling of jute fibre wastes to prepare nanocellulose, World J. Eng. 9 (2012) 45–50.
[46] M.R.K. Sofla, R.J. Brown, T. Tsuzuki, T.J. Rainey, A comparison of cellulose nanocrystals and cellulose nanofibres extracted from bagasse using acid and ball milling methods, Adv. Nat. Sci. Nanosci. Nanotechnol. 7 (2016), https://doi.org/10.1088/2043-6262/7/3/035004.
[47] A.N. Frone, D.M. Panaitescu, I. Chiulan, C.A. Nicolae, Z. Vuluga, C. Vitelaru, C.M. Damian, The effect of cellulose nanofibers on the crystallinity and nanostructure of poly(lactic acid) composites, J. Mater. Sci. 51 (2016) 9771–9791, https://doi.org/10.1007/s10853-016-0212-1.
[48] J. Stetefeld, S.A. McKenna, T.R. Patel, Dynamic light scattering: a practical guide and applications in biomedical sciences, Biophys. Rev. 8 (2016) 409–427, https://doi.org/10.1007/s12551-016-0218-6.
[49] T.T.T. Ho, T. Zimmermann, R. Hauert, W. Caseri, Preparation and characterization of cationic nanofibrillated cellulose from etherification and high-shear disintegration processes, Cellulose 18 (2011) 1391–1406, https://doi.org/10.1007/s10570-011-9591-2.
[50] L. Zhang, T. Tsuzuki, X. Wang, Preparation of cellulose nanofiber from softwood pulp by ball milling, Cellulose 22 (2015) 1729–1741, https://doi.org/10.1007/s10570-015-0582-6.
[51] R. Prathapan, R. Thapa, G. Garnier, R.F. Tabor, Modulating the zeta potential of cellulose nanocrystals using salts and surfactants, Colloids Surf. A Physicochem. Eng. Asp. 509 (2016) 11–18, https://doi.org/10.1016/j.colsurfa.2016.08.075.
[52] Y. Xu, A.D. Atrens, J.R. Stokes, Rheology and microstructure of aqueous suspensions of nanocrystalline cellulose rods, J. Colloid Interface Sci. 496 (2017) 130–140, https://doi.org/10.1016/j.jcis.2017.02.020.
[53] S. Naduparambath, J. T.V, V. Shaniba, S. M.P, A.K. Balan, E. Purushothaman, Isolation and characterisation of cellulose nanocrystals from sago seed shells, Carbohydr. Polym. 180 (2018) 13–20, https://doi.org/10.1016/j.carbpol.2017.09.088.
[54] A. Pappu, M. Saxena, V.K. Thakur, A. Sharma, Facile extraction, processing and characterization of biorenewable sisal fibers for multifunctional applications, J. Macromol. Sci. Part A 1325 (2016), https://doi.org/10.1080/10601325.2016.1176443.
[55] A.C. Corrêa, E.M. Teixeira, L.A. Pessan, L.H.C. Mattoso, Cellulose nanofibers from curaua fibers, Cellulose 17 (2010) 1183–1192, https://doi.org/10.1007/s10570-010-9453-3.
[56] C. Brinatti, J. Huang, R.M. Berry, K.C. Tam, W. Loh, Structural and energetic studies on the interaction of cationic surfactants and cellulose nanocrystals, Langmuir 32 (2016) 689–698, https://doi.org/10.1021/acs.langmuir.5b03893.
[57] A. Kaboorani, B. Riedl, Surface modification of cellulose nanocrystals (CNC) by a cationic surfactant, Ind. Crops Prod. 65 (2015) 45–55, https://doi.org/10.1016/j.indcrop.2014.11.027.
[58] H. Lu, Y. Gui, L. Zheng, X. Liu, Morphological, crystalline, thermal and physicochemical properties of cellulose nanocrystals obtained from sweet potato residue, Food Res. Int. J. 50 (2013) 121–128, https://doi.org/10.1016/j.foodres.2012.10.013.

[59] W. Chen, H. Yu, Y. Liu, P. Chen, M. Zhang, Y. Hai, Individualization of cellulose nanofibers from wood using high-intensity ultrasonication combined with chemical pretreatments, Carbohydr. Polym. 83 (2011) 1804–1811, https://doi.org/10.1016/j.carbpol.2010.10.040.

[60] R. Avolio, I. Bonadies, D. Capitani, M.E. Errico, G. Gentile, M. Avella, A multi-technique approach to assess the effect of ball milling on cellulose, Carbohydr. Polym. 87 (2012) 265–273, https://doi.org/10.1016/j.carbpol.2011.07.047.

[61] M.E. Achaby, Z. Kassab, A. Barakat, A. Aboulkas, Alfa fibers as viable sustainable source for cellulose nanocrystals extraction: application for improving the tensile properties of biopolymer nanocomposite films, Ind. CropsProd. 112 (2018) 499–510, https://doi.org/10.1016/j.indcrop.2017.12.049.

[62] S. Barazzouk, C. Daneault, Amino acid and peptide immobilization on oxidized nanocellulose: spectroscopic characterization, Nanomaterials 2 (2012) 187–205, https://doi.org/10.3390/nano2020187.

[63] E. Espinosa, J. Domínguez-Robles, R. Sánchez, Q. Tarrés, A. Rodríguez, The effect of pre-treatment on the production of lignocellulosic nanofibers and their application as a reinforcing agent in paper, Cellulose 24 (2017) 2605–2618, https://doi.org/10.1007/s10570-017-1281-2.

[64] C. Xu, S. Zhu, C. Xing, D. Li, N. Zhu, H. Zhou, Isolation and properties of cellulose nanofibrils from coconut palm petioles by different mechanical process, PLoS One 10 (2015) 1–11, https://doi.org/10.1371/journal.pone.0122123.

[65] N. Rambabu, S. Panthapulakkal, M. Sain, A.K. Dalai, Production of nanocellulose fibers from pinecone biomass: Evaluation and optimization of chemical and mechanical treatment conditions on mechanical properties of nanocellulose films, Ind. Crops Prod. 83 (2016) 746–754, https://doi.org/10.1016/j.indcrop.2015.11.083.

[66] Y.M. Zhou, S.Y. Fu, L.M. Zheng, H.Y. Zhan, Effect of nanocellulose isolation techniques on the formation of reinforced poly(vinyl alcohol) nanocomposite films, Express Polym. Lett. 6 (2012) 794–804, https://doi.org/10.3144/expresspolymlett.2012.85.

[67] M.F. Rosa, E.S. Medeiros, J.A. Malmonge, K.S. Gregorski, D.F. Wood, L.H.C. Mattoso, G. Glenn, W.J. Orts, S.H. Imam, Cellulose nanowhiskers from coconut husk fibers: Effect of preparation conditions on their thermal and morphological behavior, Carbohydr. Polym. 81 (2010) 83–92, https://doi.org/10.1016/j.carbpol.2010.01.059.

[68] S. Shankar, J.W. Rhim, Preparation of nanocellulose from micro-crystalline cellulose: The effect on the performance and properties of agar-based composite films, Carbohydr. Polym. 135 (2016) 18–26, https://doi.org/10.1016/j.carbpol.2015.08.082.

[69] T.F. Meyabadi, F. Dadashian, G. Mir Mohamad Sadeghi, H. Ebrahimi Zanjani Asl, Spherical cellulose nanoparticles preparation from waste cotton using a green method, Powder Technol. 261 (2014) 232–240, https://doi.org/10.1016/j.powtec.2014.04.039.

[70] J.C. Chandra, N. George, S.K. Narayanankutty, Isolation and characterization of cellulose nanofibrils from arecanut husk fibre, Carbohydr. Polym. 142 (2016) 158–166, https://doi.org/10.1016/j.carbpol.2016.01.015.

[71] C. Liu, B. Li, H. Du, D. Lv, Y. Zhang, G. Yu, X. Mu, H. Peng, Properties of nanocellulose isolated from corncob residue using sulfuric acid, formic acid, oxidative and mechanical methods, Carbohydr. Polym. 151 (2016) 716–724, https://doi.org/10.1016/j.carbpol.2016.06.025.

[72] G. Chauve, J. Bras, Industrial Point of View of Nanocellulose Materials and Their Possible Applications, Https://Umaine.Edu/Pdc/Cellulose-Nanomaterials/Order-Nanocellulose/, (2014), pp. 233–252, https://doi.org/10.1142/97898145664690014.

[73] T.P.D.C. of the U. of Maine, Order nanocellulose, Https://Umaine.Edu/Pdc/Cellulose-Nanomaterials/Order-Nanocellulose/, (2018), pp. 4–5 https://umaine.edu/pdc/cellulose-nano-crystals/.

[74] J. Miller, Nanocellulose State of The Industry, (2015).

[75] F. Piccinno, R. Hischier, S. Seeger, C. Som, Predicting the environmental impact of a future nanocellulose production at industrial scale: application of the life cycle assessment scale-up framework, J. Clean. Prod. 174 (2018) 283–295, https://doi.org/10.1016/j.jclepro.2017.10.226.